

## Supporting Information

### Sustainable Protection of Natural Liquid Enables Ultra-Stable Inverted Perovskite Solar Cells via Allylic Disulfide Rearrangement

Yang Yang,<sup>a#</sup> Shuyuan Wan,<sup>a#</sup> Hang Wei,<sup>a</sup> Lijun Yang,<sup>c</sup> Zhiyuan Dai,<sup>a</sup> Haoze Lu,<sup>a</sup> Zhe Liu,<sup>a</sup> Bo Chen,<sup>c</sup> Ruihao Chen,<sup>\*a,b</sup> Hongqiang Wang<sup>\*a</sup>

**Keywords:** Natural liquid, Diallyl disulfide, Chemical rearrangement, Inverted perovskites solar cells, Durable stability

a. State Key Laboratory of Solidification Processing, Center for Nano Energy Materials, School of Materials Science and Engineering, Northwestern Polytechnical University, Xi'an 710072, China

b. Research & Development Institute of Northwestern Polytechnical University in Shenzhen, 518063, China

c. National Key Laboratory for Mechanical Behavior of Materials, Xi'an Jiaotong University, Xi'an, 710049, China

\* Corresponding authors.

E-mail: hongqiang.wang@nwpu.edu.cn, rhchen@nwpu.edu.cn

## General information

### Materials

Fluorine doped tin oxide coated (FTO) glasses ( $14\ \Omega/\text{sq}$ ) were purchased from Advanced Election Technology Co., Ltd. Methylammonium iodide (MAI, 99.5%), cesium iodide (CsI, 99.5%), methylammonium chloride (MACl, 99.5%), lead iodide ( $\text{PbI}_2$ , >99.5%) and formamidinium iodide (FAI, 99.5%), were purchased from Xi'an Yuri Solar Co., Ltd. [2-(3,6-Dimethoxy-9H-carbazol-9-yl) ethyl]phosphonic Acid (MeO-2PACz, 99.5%) were purchased from TCI.  $\text{C}_{60}$  and BCP were obtained from were purchased from Vizuchem Co., Ltd. Dimethylformamide (DMF, 99.8%), dimethyl sulfoxide (DMSO, 99.8%), 2-Methoxyethanol (2-Me, 99.8%), ethyl acetate (EA, 99.8%) from Alfa Aesar Chemical Co., Ltd. Diallyl disulfide (DAD) were purchased from Beijing InnoChem Science & Technology Co., Ltd.

### Fabrication of PSCs and modules

FTO glass substrate was washed sequentially by detergent, deionized water, acetone and ethanol for 25 min with ultrasound devices. The cleaned substrate was dried in the drying cabinet for 2 h and treated by plasma for 20 min, then transferred into a nitrogen glove box quickly. The MeO-2PACz (0.5 mg/mL in 2-Me) was fabricated on the FTO substrate by spin-coating at 3000 rpm for 30 s, followed by annealing at  $100\ ^\circ\text{C}$  for 10 min. The perovskite precursor solution was prepared by dissolving completely 1.5 M  $\text{Cs}_{0.05}\text{MA}_{0.10}\text{FA}_{0.85}\text{PbI}_3$  (in which FAI, MAI, FAI, CsI,  $\text{PbI}_2$  and excess MACl (5 mol%) with and without DAD) in a mixed solvent of DMF and DMSO with a volume ratio of 4:1. The 70  $\mu\text{L}$  of perovskite precursor was spin-coated onto HTL at 1000 rpm for 10 s and 5000 rpm for 30 s respectively and 150  $\mu\text{L}$  EA was dropped on the film at 5 s before the end of procedure (spin coater from Jiangyin J. Wanjia Technology Co., Ltd.). After that the film was annealed at  $120\ ^\circ\text{C}$  for 20 min and completely cooled.  $\text{C}_{60}$  (25 nm) and BCP (8 nm) was thermally evaporated in a vacuum chamber ( $\leq 5 \times 10^{-4}$  Pa). Finally, Ag electrode (80 nm) was deposited by thermal evaporation in a vacuum chamber ( $\leq 5 \times 10^{-4}$  Pa). All these processes were conducted in the glove box protected by  $\text{N}_2$  with  $\text{O}_2$  and  $\text{H}_2\text{O}$  contents kept below 0.01 ppm.

The scalability of the DAD molecule for defect passivation and dynamic healing was validated by fabricating the  $6 \times 6\ \text{cm}^2$  inverted module. 250  $\mu\text{L}$  perovskite precursor solution (DAD, 0.75 mg/mL) was drop-cast onto a substrate coated with a hole transport layer at 6000 rpm for 30 s,

followed by the addition of 400  $\mu\text{L}$  of antisolvent EA during the last 5 s of the process. The wet film was then transferred to a hotplate and annealed at 120  $^{\circ}\text{C}$  for 30 min. Next,  $\text{C}_{60}$  (25 nm), BCP (8 nm), and Cu (150 nm) were sequentially deposited via thermal evaporation under high vacuum ( $\leq 5 \times 10^{-4}$  Pa). The laser scribing process followed the parameters shown in Fig. S33, resulting in a large-area module with an aperture area 26.78  $\text{cm}^2$  and a geometrical fill factor (GFF) of 96.3%.

## Characterization

Fourier transform infrared (FTIR) data were gained by a FTIR spectrometer (Bruker, Tensor II). The Raman data were obtained from Thermo DXR2xi. Ultraviolet-visible (UV-vis) spectra were obtained by a UV-vis spectrometer (Shimadzu UV-2550). The top-view images of perovskite samples and cross-sectional images of devices were monitored by scanning electron microscopy (SEM, Hitachi Regulus8100). Depth resolved GIXRD were characterized using a Rigaku Smart Lab five-axis X-ray diffractometer at 45 kV and 200 mA, equipped with Cu  $\text{K}\alpha$  radiation ( $\lambda = 1.54050$  Å), parallel beam optics and a secondary graphite monochromator. X-ray photoelectron spectroscopy (XPS) and Ultraviolet Photoelectron Spectroscopy (UPS) data were collected by a Axis Ultra DLD Kratos AXIS SUPRA. The Photoluminescence (PL) and time-resolved photoluminescence (TRPL) spectra were obtained by a Pico Quant Fluo Time 300 fluorescence spectrometer. The external quantum efficiency (EQE) of devices was measured by an Enlitech EQE measurement system (CEL-QPCE1000).  $J$ - $V$  curves characteristics were measured using solar simulator (Oriel 67005, 150 W) with irradiation intensity of 100  $\text{mW cm}^{-2}$  AM 1.5G standard light.  $J$ - $V$  curves characteristics of perovskite modules were measured using solar simulator (Newport, 94063A) with irradiation intensity of 100  $\text{mW cm}^{-2}$  AM 1.5G standard light. The electrochemical workstation (Chenhua CHI660E) was employed to obtain electrochemical impedance spectroscopy (EIS) and Mott-Schottky (MS) analysis. The *in-situ* X-ray diffraction profile was gained from Bruker D8 Advance instrument and technology Ltd. The 3<sup>rd</sup> Synchrotron radiation light source was used for glancing incidence wide-angle X-ray scattering (GIWAXS). The conductive atomic force microscopy (C-AFM, Bruker Dimension ICON) was taken to obtain the current mapping image. The particle size distribution of the precursor solution was obtained by dynamic light scattering (DLS, Malvern Zetasizer Nano ZS90). TOF-SIMS (Tescan AMBER) spectrometer was used for depth profile analysis of perovskites with 30 KV and 30 pA. The operational stability tests for the

unencapsulated PSCs were performed at the maximum power point (MPP) under constant illumination using a 1-sun equivalent white-light LED array (Multi-Channels Solar Cells Stability Test System, Wuhan 91PVKSolar Technology Co. Ltd, China). For the P1-P3 laser-patterning lines were according to our previous works.<sup>1-3</sup> Transient photovoltage (TPV) and transient photocurrent (TPC) for PSCs were measured using a ZAHNE MESSSYSTEME (Instrument model: PP211).

## **DFT Calculation**

The computational framework utilized in this study is based on first-principles density functional theory (DFT) calculations. Specifically, the Perdew-Burke-Ernzerhof (PBE) exchange-correlation functional under the generalized gradient approximation (GGA) is employed. Self-consistency of the electronic energy is achieved when the energy variation falls below  $10^{-5}$  eV. For the evaluation of defect and adsorption energies, the  $\text{PbI}_2$ -terminated supercell is expanded to a  $3 \times 3 \times 1$  configuration, with the energy cutoff adjusted to 500 eV. A force tolerance of  $0.03 \text{ eV } \text{\AA}^{-1}$  is enforced during simulations. To prevent artificial interactions, a vacuum layer of 30  $\text{\AA}$  is introduced perpendicular to the structural plane for surface models. The geometry optimization proceeds until the energy variation per atom stabilizes below  $0.05 \text{ eV } \text{\AA}^{-1}$ , ensuring structural convergence.<sup>4-5</sup>

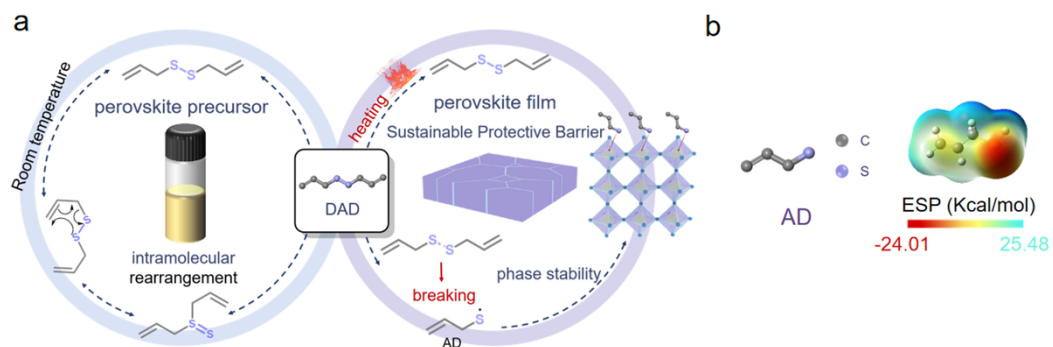


**Fig. S1.** (a) Schematic diagram of the intramolecular chemical rearrangement process. (b) Chemical structure and electrostatic potential energy of AD molecule.

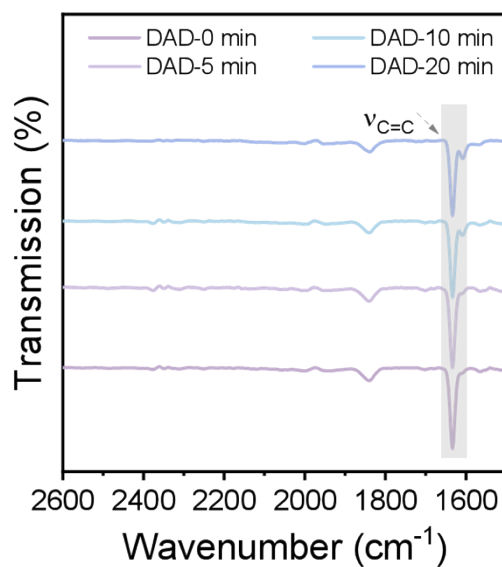


**Fig. S2.** FTIR spectra of the DAD liquid before and after anneal with different duration.

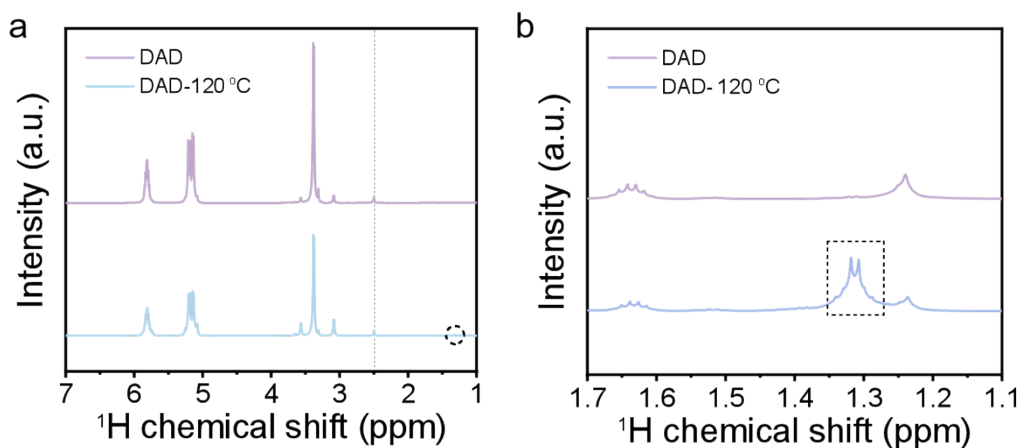
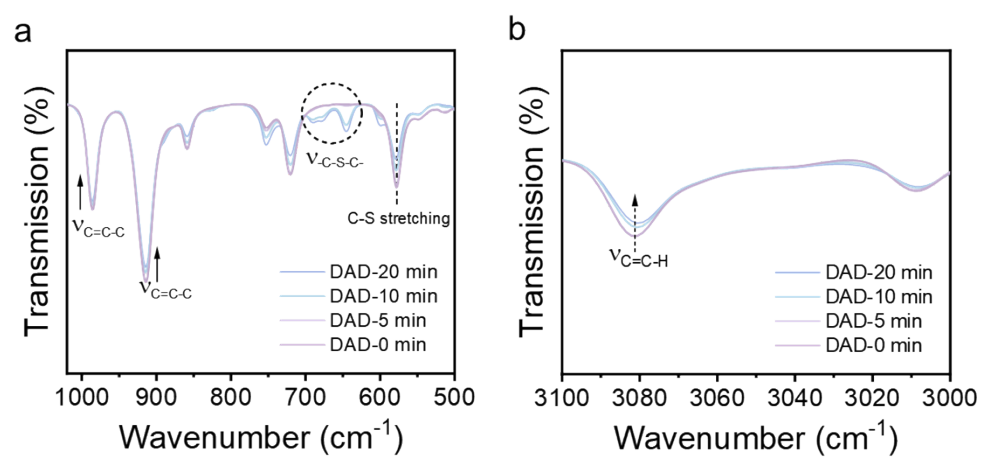


**Fig. S3.** (a) Full and (b) regional  $^1\text{H}$  NMR spectra of DAD before and after anneal with 20 min.



**c**

Reaction process:

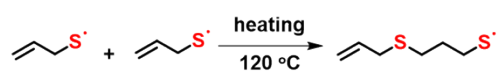


**Fig. S4.** (a) and (b) regional FITR spectra of DAD after anneal for different duration. (c) Chemical reaction of DAD during heating process derived from  $^1\text{H}$  NMR and FITR analysis.

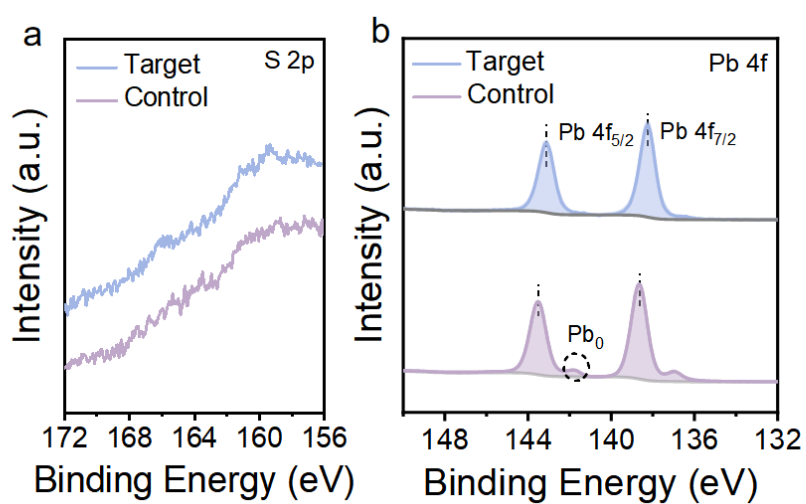


**Fig. S5.** XPS spectra of (a) S 2p and (b) Pb 4f peaks of the control and target perovskite films. The signal of S element was detected in the target film with DAD additive. And Pb 4f XPS peaks shifted toward lower binding energies in the target film compared to the control film.

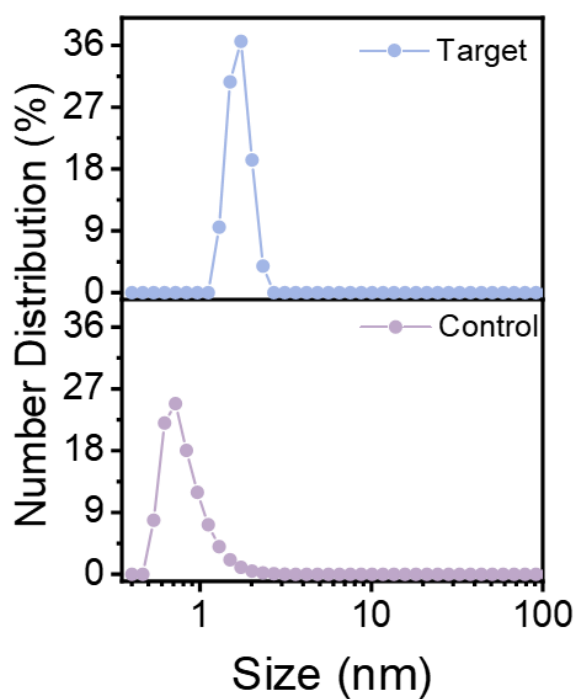


**Fig. S6.** Particle size distribution of the control and target perovskite precursor solution.

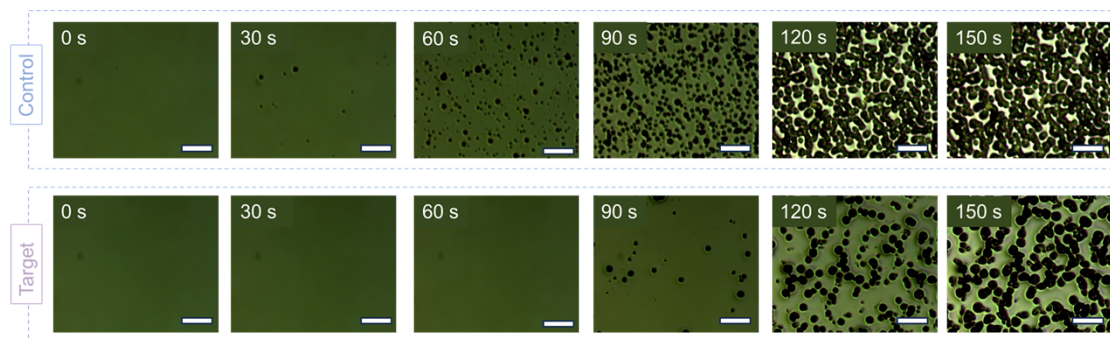


**Fig. S7.** Optical microscope images of solvent-free wet control and target films at different stages (scale of 10  $\mu\text{m}$ ).

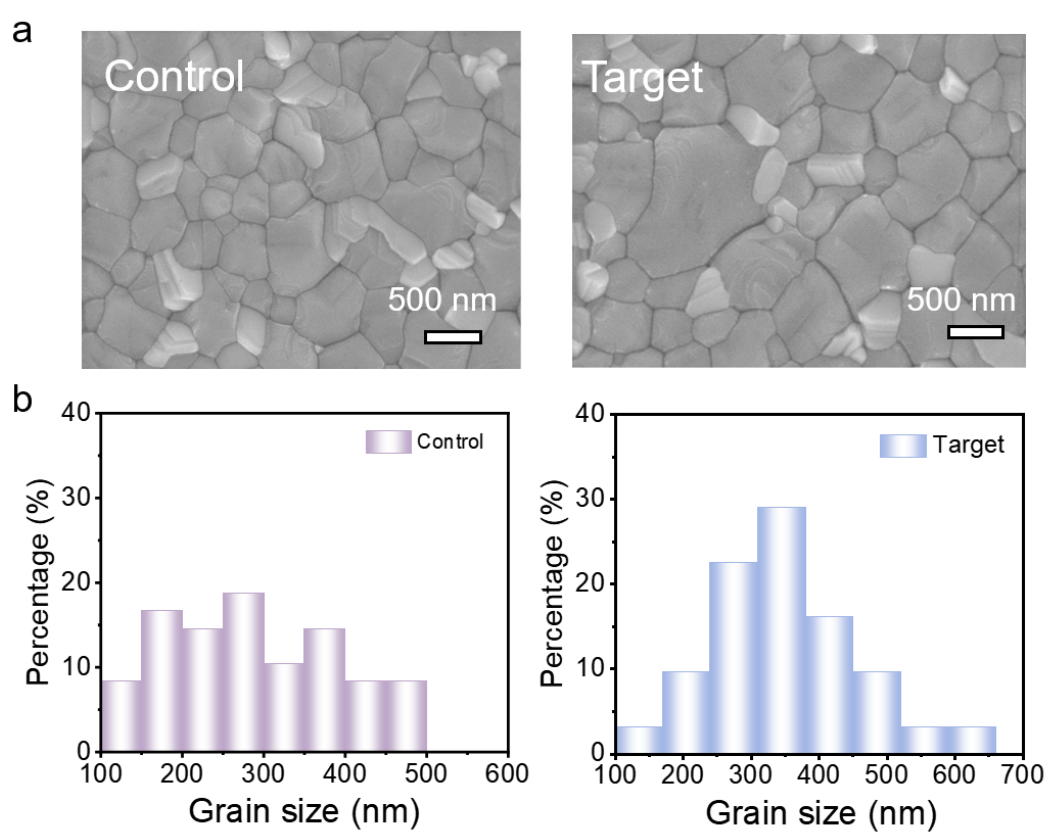


**Fig. S8.** (a) Surface SEM images and (b) corresponding grain size distribution of the control and target films.



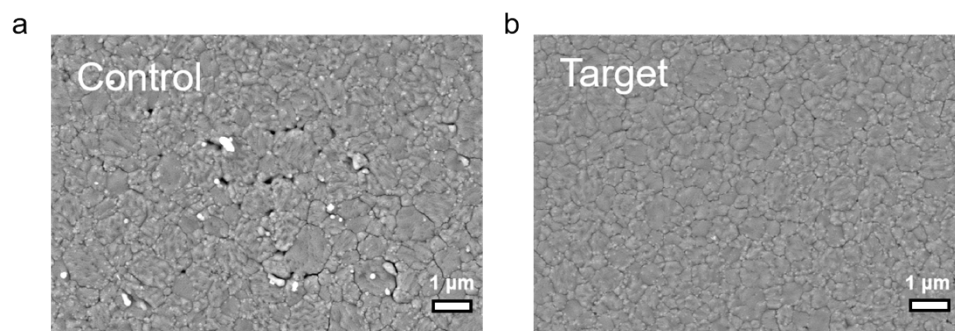


**Fig. S9.** SEM images of the buried interface of the (a) control and (b) target films.

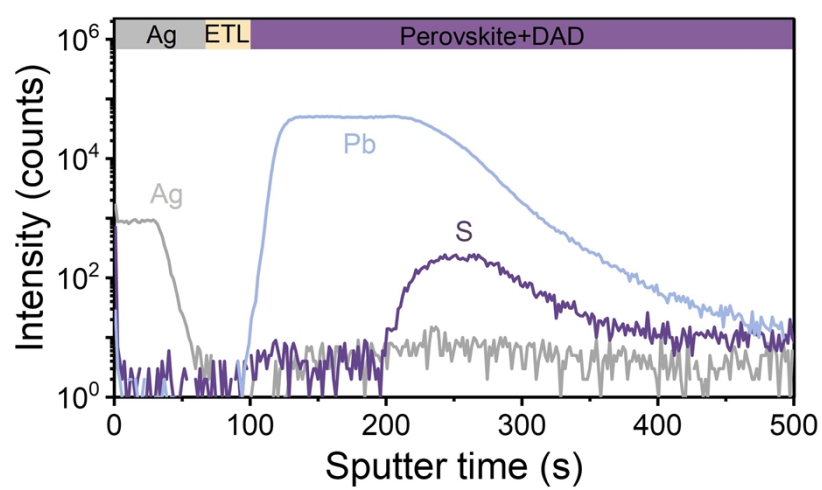


**Fig. S10.** TOF-SIMS measurement of the target perovskite solar cells.

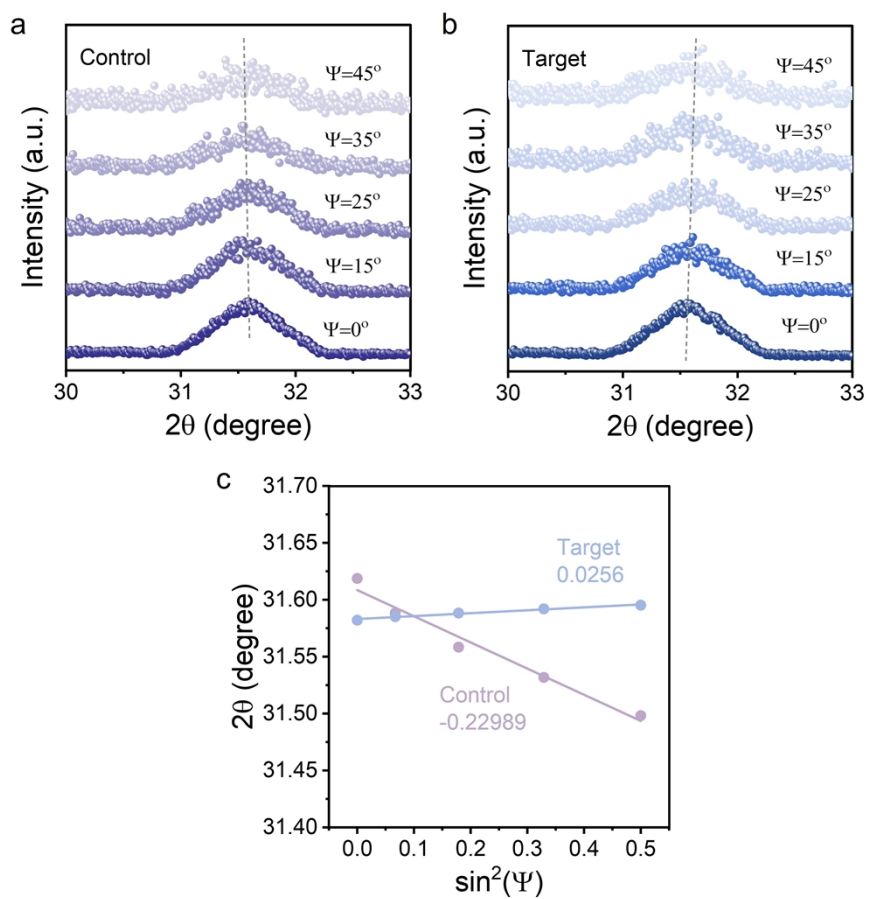


**Fig. S11.** GIXRD patterns of the (a) control and (b) target. (c) Linear fitting of the stress distribution of the control and target films versus  $\sin^2(\Psi)$ .

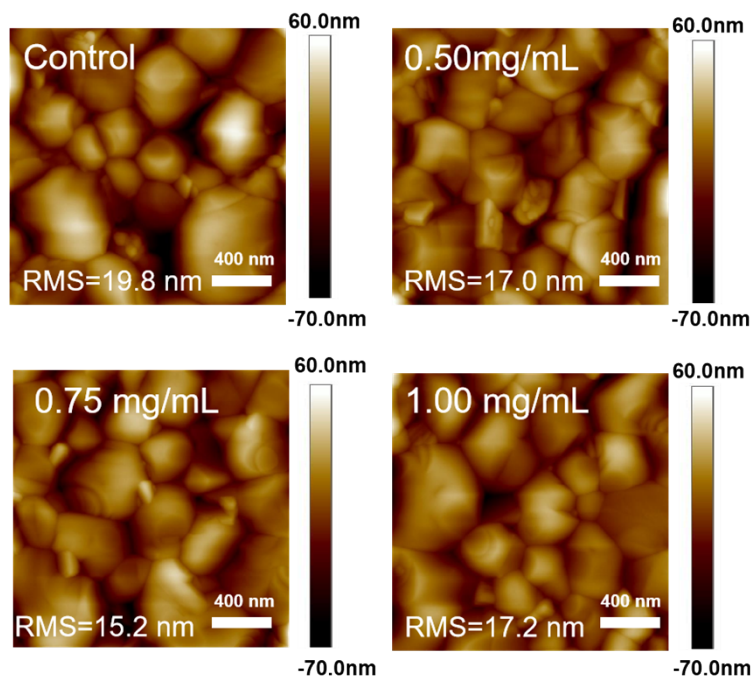


**Fig. S12.** AFM images of the control and perovskite films with different concentrations of DAD (0.50 mg/mL, 0.75 mg/mL, and 1.00 mg/mL).

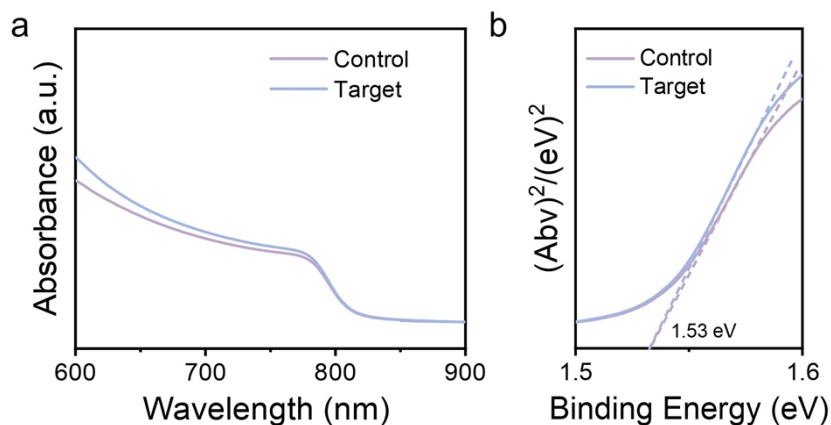


**Fig. S13.** (a) UV-vis absorption spectra of the control and target perovskite films. (b) Tauc plot for the control and perovskite films. The optical bandgap of perovskite is 1.53 eV. This result suggests that adding a small amount of DAD does not impact the bandgap, confirming that the increased light absorption is primarily due to better crystallinity rather than changes in the electronic structure.

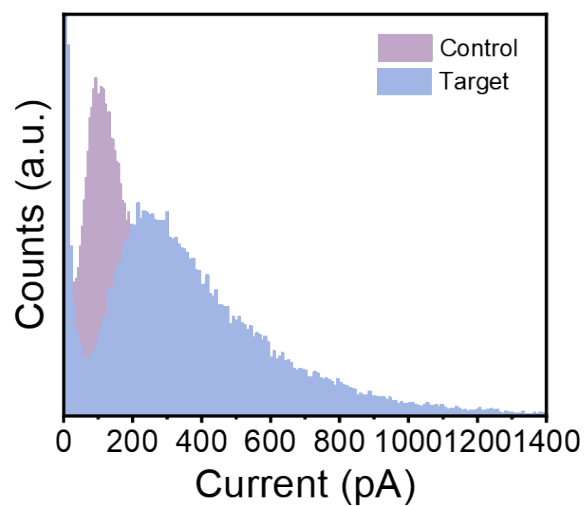


**Fig. S14.** Corresponding current curves of the control and target perovskite films derived from Fig. 2g, h.

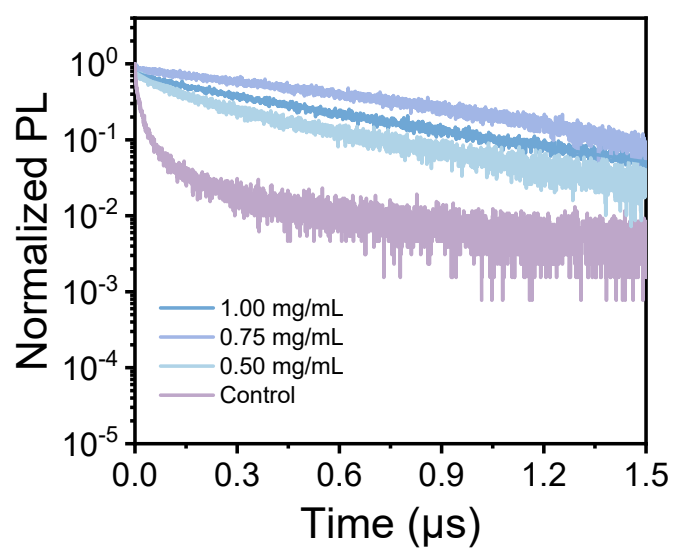


**Fig. S15.** TRPL spectra of the control and perovskite films with different concentrations of DAD (0.50 mg/mL, 0.75 mg/mL, and 1.00 mg/mL). The detailed parameters are provided in Table S1.

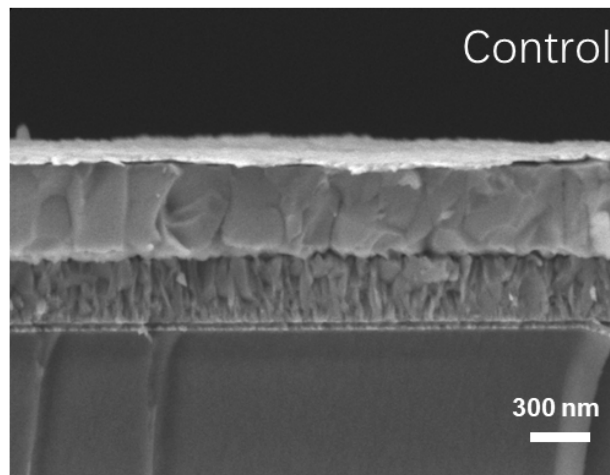


**Fig. S16.** SEM cross-sectional image of the control device.

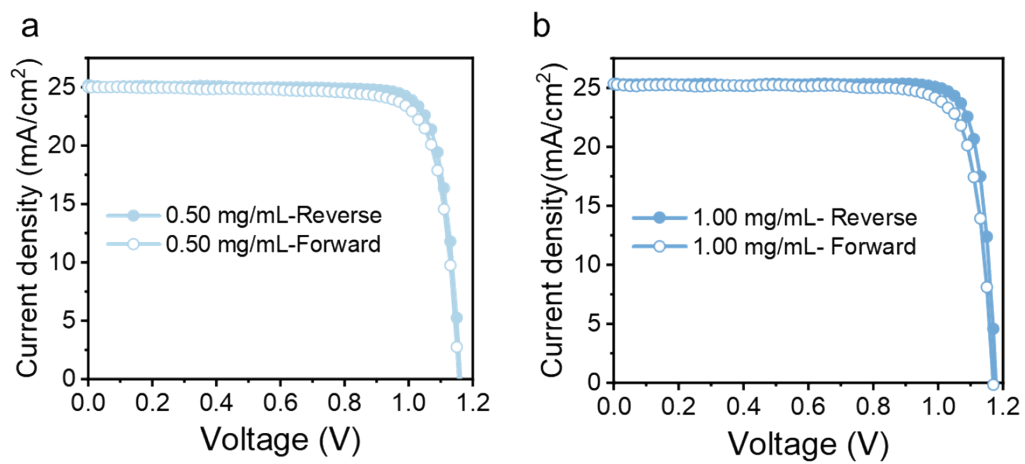


**Fig. S17.** Forward and reverse  $J$ - $V$  scans of PSCs with (a) 0.50 mg/mL and (b) 1.00 mg/mL DAD.

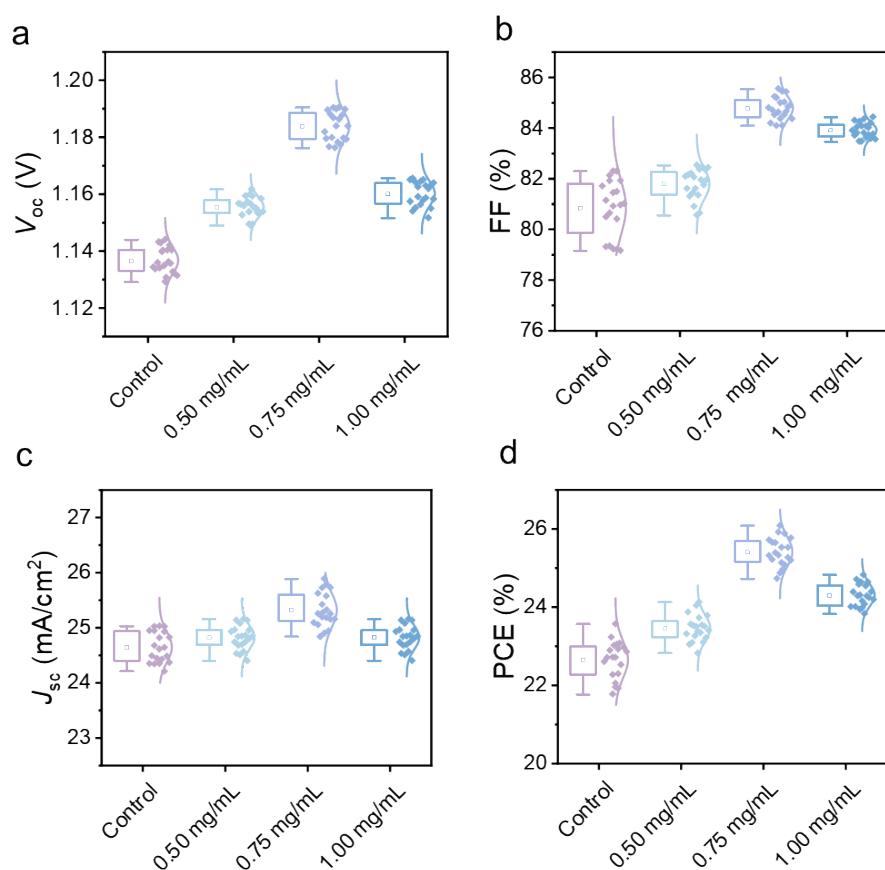


**Fig. S18.** Statistical box for open-circuit voltage ( $V_{oc}$ ), fill factor (FF), short-circuit current densities ( $J_{sc}$ ), power conversion efficiency (PCE) of the control and PSCs with different concentrations of DAD.

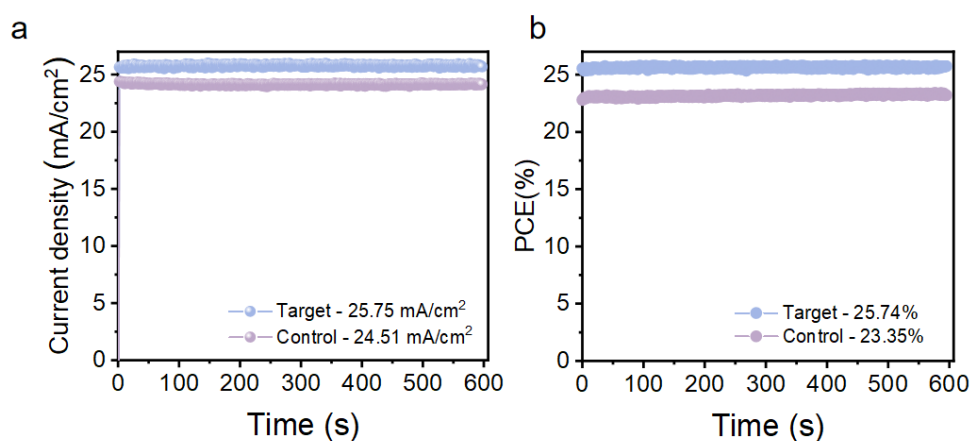


**Fig. S19.** (a) Photocurrent outputs and (b) Stabilized PCEs at the maximum output power point of the control and target PSCs (0.75 mg/mL).

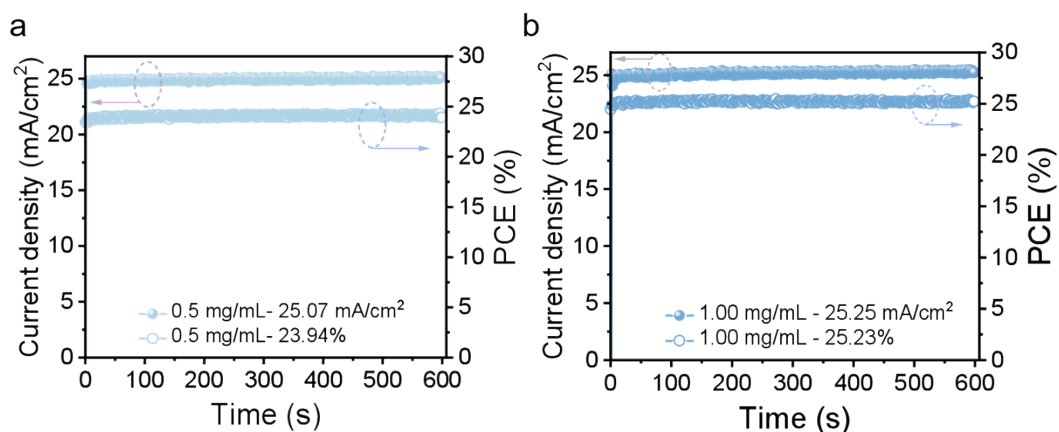


**Fig. S20.** Photocurrent outputs and Stabilized PCEs at the maximum output power point of the PSCs with (a) 0.50 mg/mL and (b) 1.00 mg/mL DAD.



中国认可  
国际互认  
检测  
CALIBRATION  
CNAS L0641



## 检测报告

Test Report

报告编号:  
Report No. JLY20250197W

样品名称 Sample Name	钙钛矿太阳能电池 Perovskite solar cells
委托单位 Name of Client	西北工业大学 Northwestern Polytechnical University
生产单位 Manufacturer	/

天津市计量监督检测科学研究院  
Tianjin Institute of Metrological Supervision and Testing



**Fig. S21.** Efficiency certification report of the target perovskite solar cell. The testing agency is Tianjin Institute of Metrological Supervision and Testing, China.

天津市计量监督检测科学研究院  
Tianjin Institute of Metrological Supervision and Testing  
检测报告  
Test Report

报告编号: JLY20250197W 共 4 页 第 1 页  
Report No. Page No. 4-1

样品名称 Sample Name	钙钛矿太阳能电池 Perovskite solar cells				
规格型号 Specification Type	NPU-CRH	商标/出厂编号 Brand/Serial Number	NPU-CRH /	生产日期/批号 Produce Date/ Serial Number	/
样品等级 Sample Grade	/	样品描述 Sample Description	Good appearance , no obvious visible defects.	样品接收时间 Sample receive time	2025-03-18
委托日期 Delivery Date	2025-03-18	送样人员 Delivered by	/	样品数量 Sample Quantity	1块
委托单位名称 及联系电话 Name of Client	西北工业大学 Northwestern Polytechnical University/18250803209				
生产单位名称 Manufacturer	/				
检测时间 Test Time	2025-03-18	检测地点 Test Location	本院五号堤路院 区光伏产业计量 部106、107室	检测环境 Test Condition	温度: 25.0℃ 相对湿度: 28.9%
检测依据 Test Standard	IEC 60904-1:2020《光伏器件 第1部分: 光伏电流-电压特性的测量》				
检测结论 Test Conclusion	/ <div>天津市计量监督检测科学研究院 (Tianjin Institute of Metrological Supervision and Testing) 签发日期: 2025-03-20 Issue Date: 2025-03-20</div>				
备注 Remark	/				

编制: 周超 审核: 柳云秀 批准: 柳云秀  
Compiled by Checked by Approved by

**Fig. S22.** Efficiency certification report of the target perovskite solar cell. The testing agency is Tianjin Institute of Metrological Supervision and Testing, China.

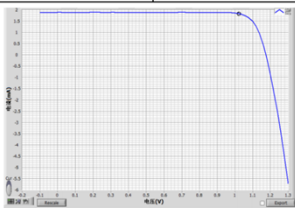


天津市计量监督检测科学研究院  
Tianjin Institute of Metrological Supervision and Testing  
检测报告

Test Report

报告编号: JLY20250197W  
Report No.

共 4 页 第 4 页  
Page No.4-4

检测项目及结果								
测试时间 Date	2025.03.18							
测试条件 Condition	使用稳态 AAA 级太阳模拟器, 在 AM1.5G, 1000W/m <sup>2</sup> , 25.0°C条件下测试 Sample was tested under the condition of AM1.5G, 1000W/m <sup>2</sup> , 25.0°C with a steady-state class calibrated AAA solar simulator							
有效面积 Active area	0.073cm <sup>2</sup> 备注: 器件的有效面积是由带固定孔径的薄金属掩模板量化。 Remark: Designated area defined by thin metal aperture mask.							
样品编号 №	V <sub>oc</sub> (V)	I <sub>sc</sub> (mA)	J <sub>sc</sub> (mA/cm <sup>2</sup> )	P <sub>max</sub> (mW)	V <sub>m</sub> (V)	I <sub>m</sub> (mA)	FF (%)	η (%)
20250197-1	1.175	1.886	25.83	1.877	1.020	1.841	84.75	25.72
测试程序 Test program settings	起始电压: Starting voltage:				+1.30V			
	终止电压: Termination voltage:				-0.10V			
	扫描间隔: Scan interval:				0.02V			
	延迟时间: Delay time:				0.01s			
I-V 曲线图 I-V curve								
备注 Remark	—							

— 以下空白 —

Blank below

**Fig. S23.** Efficiency certification report of the target perovskite solar cell. The testing agency is Tianjin Institute of Metrological Supervision and Testing, China.

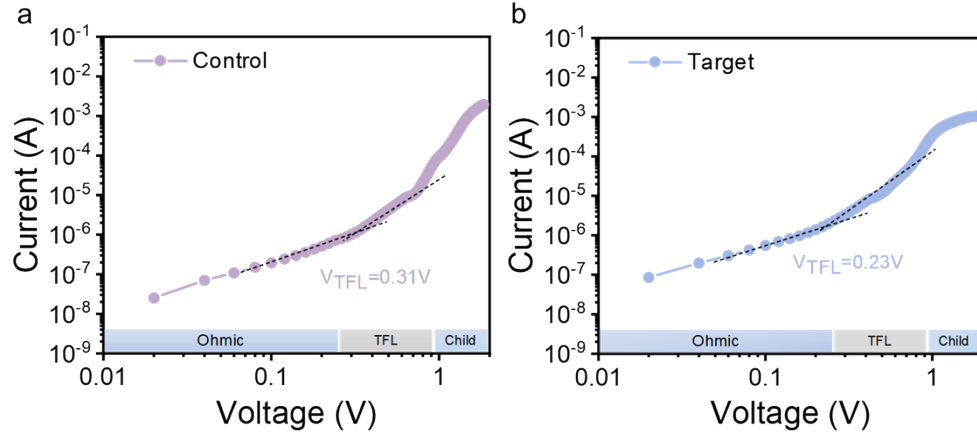


**Fig. S24.** Dark  $J$ - $V$  curves of the hole-only (a) control and (b) target devices based on SCLC mode.

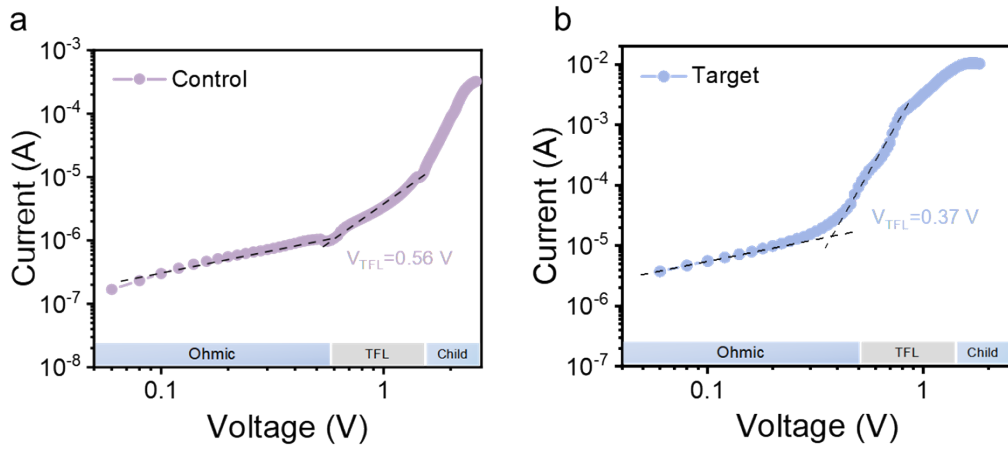


**Fig. S25.** Dark  $J$ - $V$  curves of the electron-only (a) control and (b) target devices based on SCLC mode.

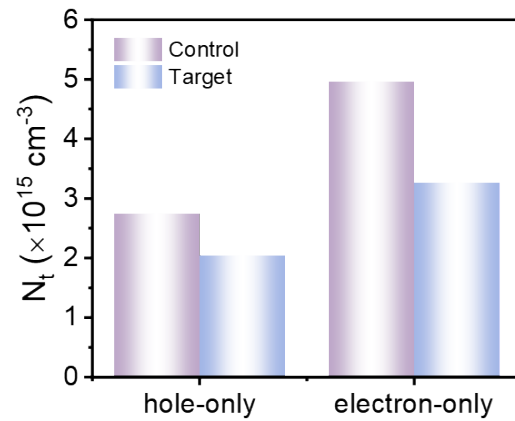


**Fig. S26.** Summary diagram of dark  $J$ - $V$  curves of the hole-only and electron-only devices based on SCLC mode.

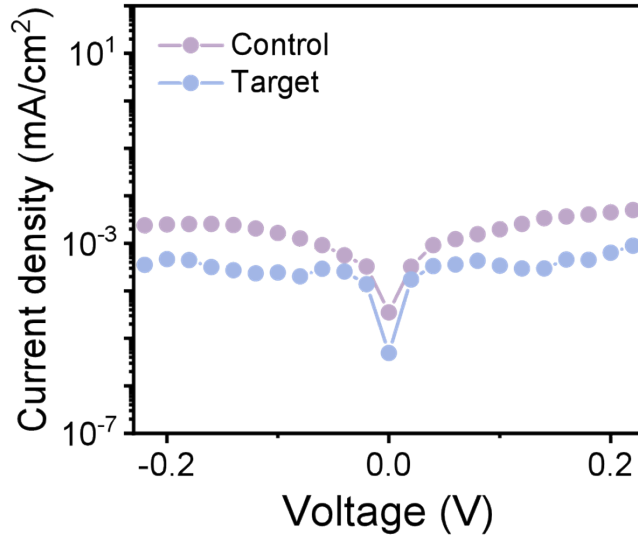


**Fig. S27.** Dark  $J$ - $V$  curves of the control and target PSCs.

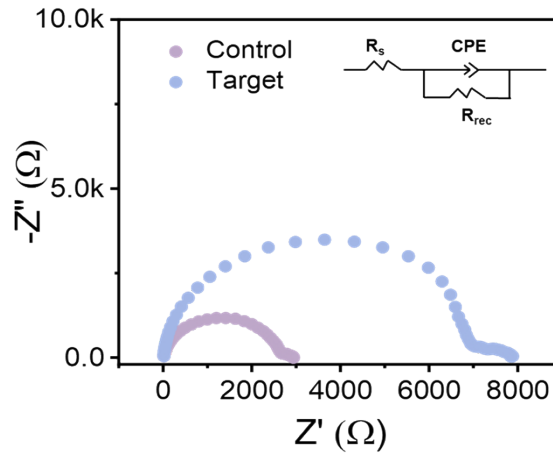


**Fig. S28.** EIS of the control and target PSCs. The detailed parameters are provided in Table S3. EIS measurements were conducted to further investigate the carrier transport and recombination processes in perovskite devices incorporating DAD. The reduced  $R_s$  improves carrier transport, while the increased  $R_{rec}$  benefits non-radiative recombination suppression.

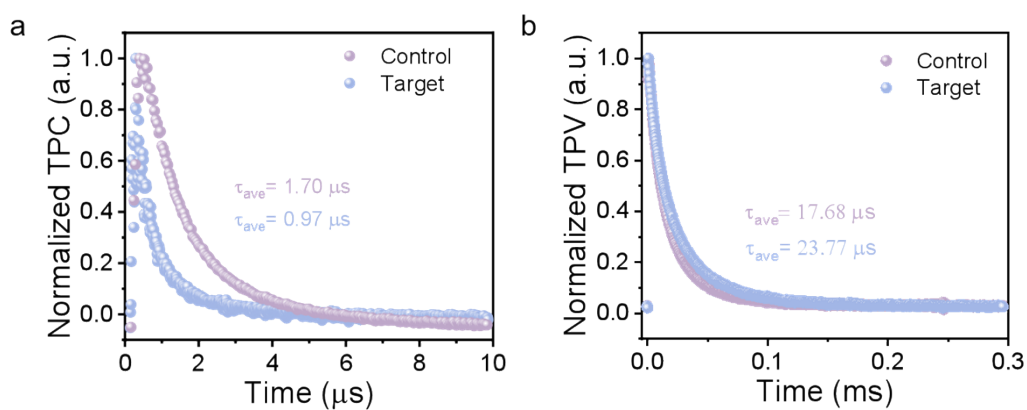


**Fig. S29.** (a) TPC and (b) TPV spectra of the control and target devices.

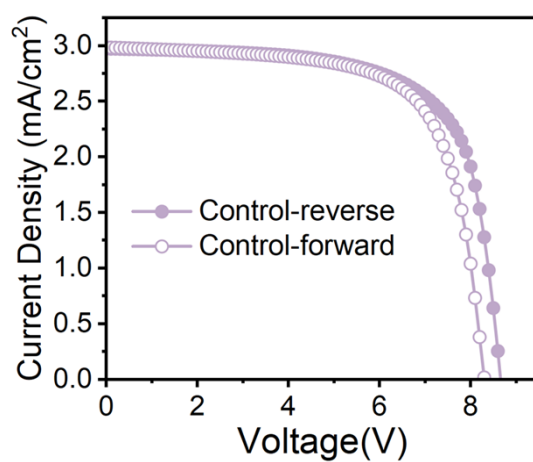


**Fig. S30.**  $J$ - $V$  scans of the control perovskite solar modules with an aperture area of 26.78 cm<sup>2</sup>.

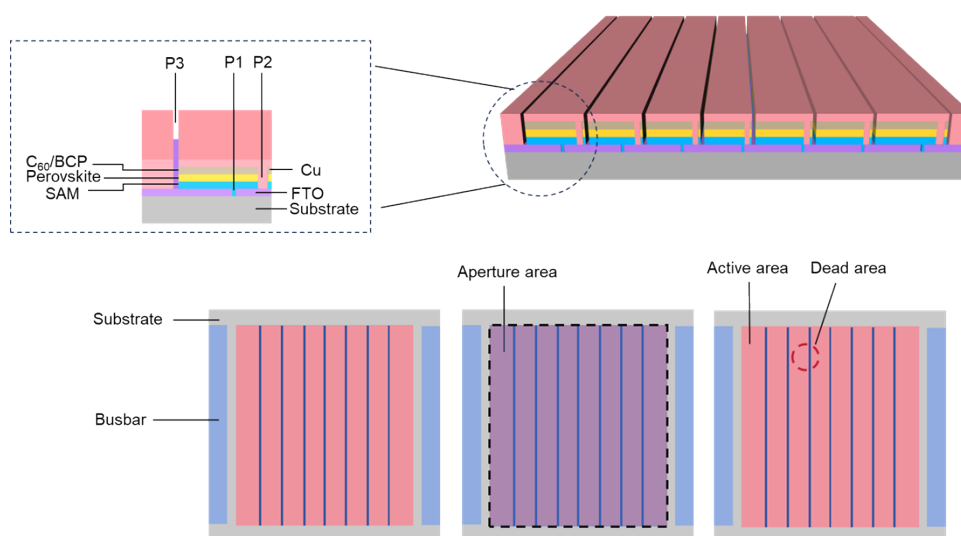


**Fig. S31.** Schematic of the perovskite solar module.<sup>1</sup>

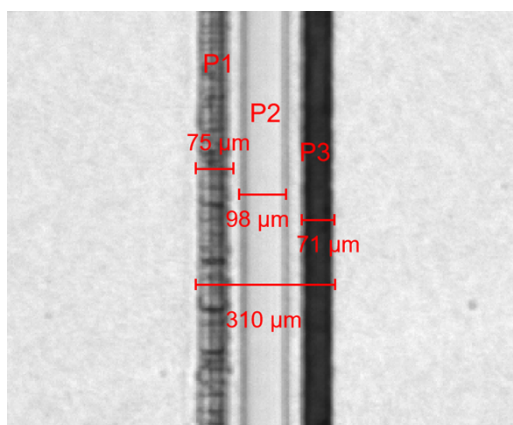


**Fig. S32.** Optical image of the PSC module with the P1-P2-P3 parameters.

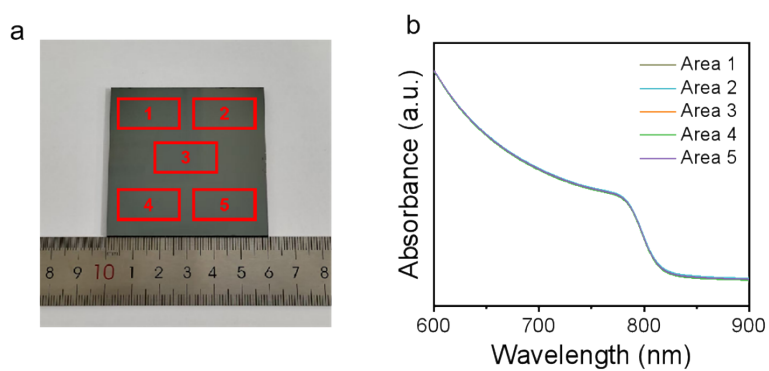


**Fig. S33.** (a) UV-vis spectra measured from five distinct regions of the 6×6 cm<sup>2</sup> film. (b) The displaying a digital photograph of the large-area perovskite film.

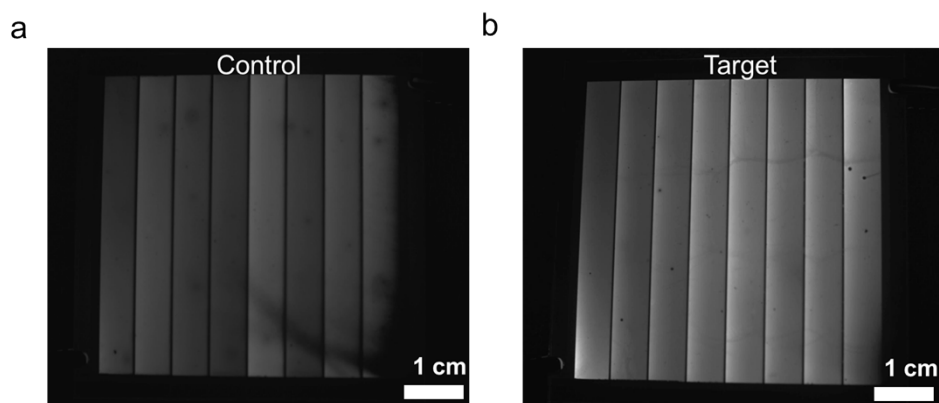


**Fig. S34.** Electroluminescence (EL) images of (a) control and (b) target PSMs.

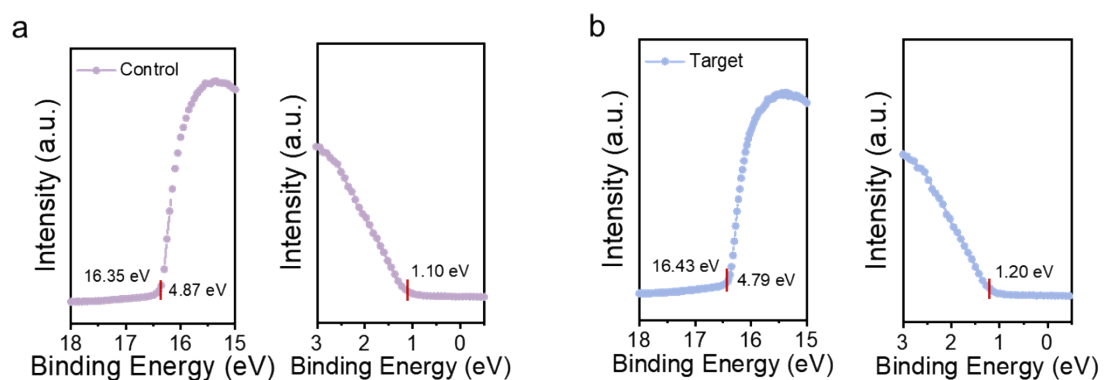


**Fig. S35.** UPS spectra of the control and target films in the (a) secondary electron cut-off region and (b) valence band region.

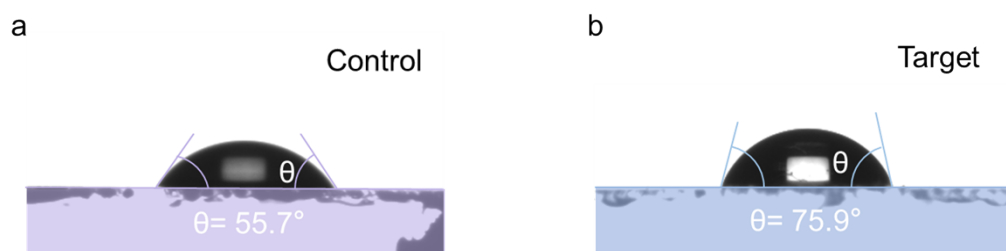


**Fig. S36.** Water contact angles of the control and target films.

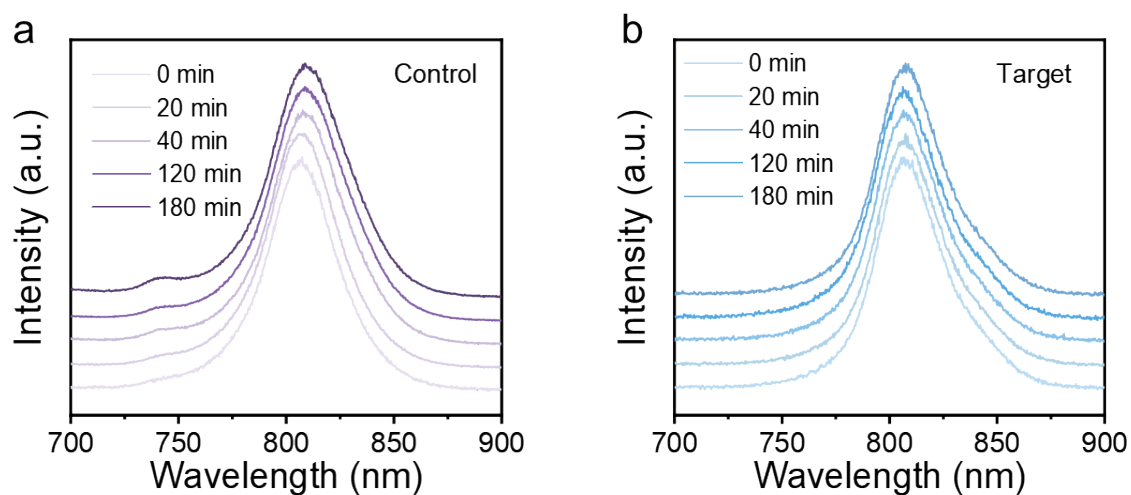


**Fig. S37.** PL spectra of the control (a) and (b) target perovskite films after different hours of 1 sun illumination (AM 1.5G) at air condition (25 °C and 35%RH).

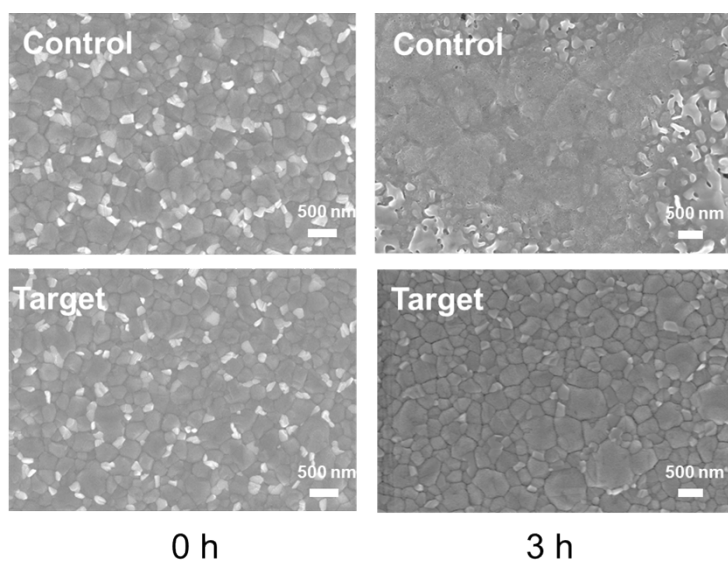


**Fig. S38.** SEM images of the control and target films after 3 h of 1 sun illumination (AM 1.5G) at air condition (25 °C and 35%RH).

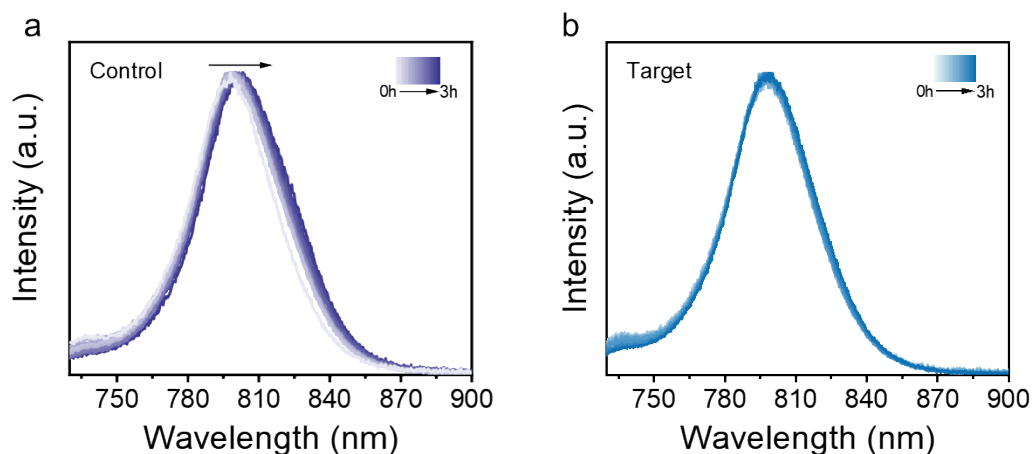


**Fig. S39.** PL spectra of the control and target films after different hours of 1 sun illumination (AM 1.5G) at high-temperature and high-relative humidity environment (85 °C and 35%RH).

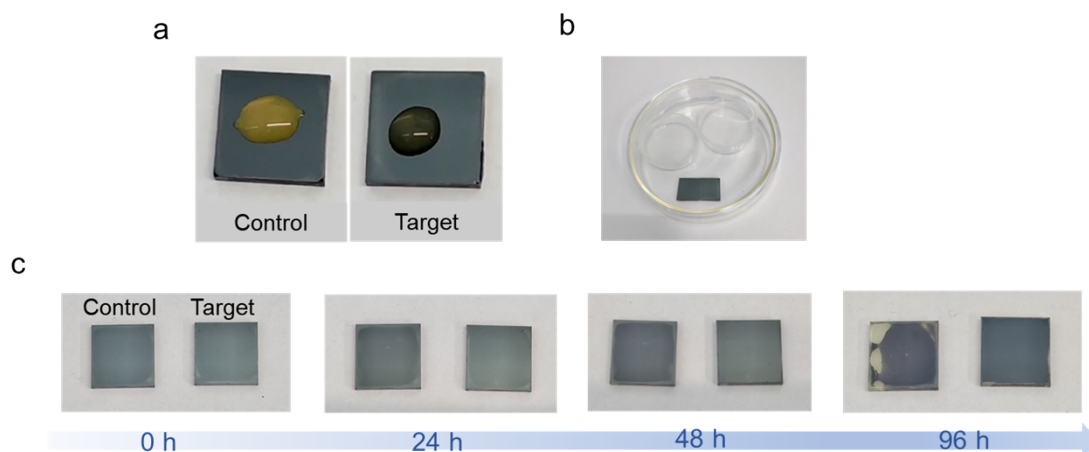


**Fig. S40.** Water resistance testing of the control and target perovskite films. As seen in Fig. S40a, water droplets were placed on the two perovskite films, the control film shows significant change, while the target film exhibits much less change. The control and target films were placed in the high-humidity environment and continuously monitored for changes. After 96 h, the target film was more stable than the control sample (Fig. S40b, c).



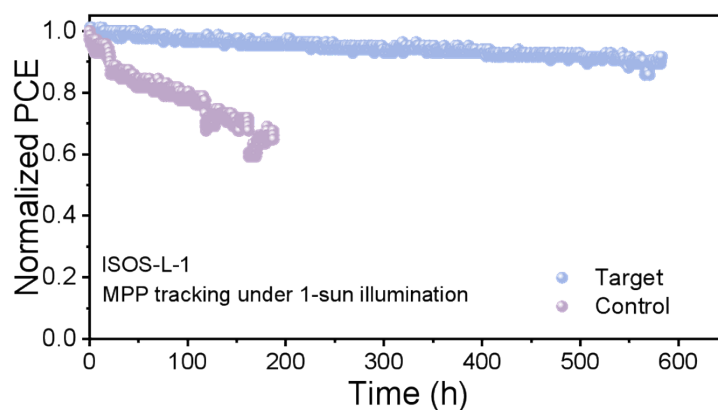


**Fig. S41.** Operation stability of the control and target PSC modules under MPP tracking.

**Table S1.** Parameters of TRPL spectra of the control and perovskite films with different concentrations of DAD (0.50 mg/mL, 0.75 mg/mL, and 1.00 mg/mL).

Structure	$A_1$ (%)	$\tau_1$ (ns)	$A_2$ (%)	$\tau_2$ (ns)	$\tau_{ave}$ (ns)
Control	44	69.0	56	116.9	101.7
0.50 mg/mL	39	74.6	61	415.1	379.7
0.75 mg/mL	5	164.3	95	1131	1123.8
1.00 mg/mL	20	80.5	80	568.7	551.7

**Table S2.** Photovoltaic parameters of the control and PSCs with different DAD concentration (0.50 mg/mL, 0.75 mg/mL, and 1.00 mg/mL).

Device		$V_{oc}/V$	$FF/\%$	$J_{sc}/mA \cdot cm^2$	$\eta/\%$
Control	Reverse	1.145	82.25	25.03	23.57
	Forward	1.132	74.80	24.99	21.16
0.50 mg/mL	Reverse	1.162	82.55	25.16	24.13
	Forward	1.156	80.17	25.02	23.19
0.75 mg/mL	Reverse	1.190	85.01	25.79	26.08
	Forward	1.182	84.16	25.63	25.49
1.00 mg/mL	Reverse	1.178	85.56	25.33	25.53
	Forward	1.170	81.25	25.33	24.08

**Table S3.** Specific values of recombination resistance ( $R_{\text{rec}}$ ) and series resistance ( $R_s$ ) for the control and target devices.

	$R_s(\Omega)$	$R_{\text{rec}}(\Omega)$
Control	25.94	1745
Target	16.06	6924

**Table S4.** Photovoltaic parameters of PSC modules (aperture area of 26.78 cm<sup>2</sup>) without or with DAD.

Device		$J_{\text{sc}}/\text{mA}\cdot\text{cm}^2$	$V_{\text{oc}}/\text{V}$	$FF/\%$	$\eta/\%$
Control	Reverse	2.97	8.66	69.25	17.83
	Forward	2.98	8.30	68.97	17.09
Target	Reverse	3.05	9.02	76.21	20.98
	Forward	3.06	8.90	75.88	20.68

#### Supplementary references

1. Y. Yang, R. Chen, J. Wu, Z. Dai, C. Luo, Z. Fang, S. Wan, L. Chao, Z. Liu and H. Wang, *Angew. Chem. Int. Ed.*, 2024, **63**, e202409689.
2. Y. Yang, S. Chen, Z. Dai, H. Wei, S. Wan, Y. Chen, J. Sun, Z. Liu, L. Ding, H. Xia, R. Chen and H. Wang, *Angew. Chem. Int. Ed.*, 2024, **64**, e202420262.
3. Y. Yang, Q. Chang, Y. Yang, Y. Jiang, Z. Dai, X. Huang, J. Huo, P. Guo, H. Shen, Z. Liu, R. Chen and H. Wang, *J. Mater. Chem. A*, 2023, **11**, 16871-16877.
4. Zhou, F., Cococcioni, M., Marianetti, C. A., Morgan, D. & Ceder, G., *Physical Review B* 70, 2004, 235121.
5. Kresse, G. & Furthmüller, J., *Comput. Mater. Sci.*, 1996, **6**, 15-50.